

## Beyond Epitaxy: Ion Implantation as a Tool for Orbital Engineering

Andreas Herklotz\*, Jonathan R. Petrie, and Thomas Z. Ward\*

Cite This: *ACS Appl. Electron. Mater.* 2025, 7, 7580–7584

Read Online

ACCESS |

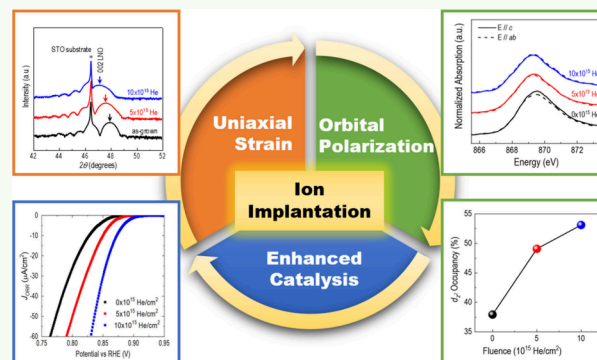
Metrics &amp; More

Article Recommendations

Supporting Information

**ABSTRACT:** Manipulating electronic orbital states in quantum materials provides a powerful means of controlling their physical properties and technological functionality. Here, we demonstrate that orbital populations in strongly correlated oxide thin films can be continuously and reversibly tuned through postsynthesis He ion implantation. Using  $\text{LaNiO}_3$  as a model system, we show that the orbital preference can be systematically adjusted from favoring in-plane  $d_{x^2-y^2}$  occupation toward out-of-plane  $d_z$  states through precise control of ion fluence. Unlike conventional heteroepitaxial approaches that lock in orbital configurations during growth, this strain-doping technique enables continuous orbital tuning and the selective modification of specific film regions after device fabrication. We demonstrate the practical impact of this control by achieving a 7-fold enhancement in oxygen reduction reaction catalysis. This work establishes ion implantation as a powerful approach for orbital engineering that complements existing synthesis-based strategies while offering unique advantages for both basic research and device development.

**KEYWORDS:** Orbital Polarization, Strain Engineering, Nickelates, Perovskites, Oxygen Reduction Reaction



## INTRODUCTION

Orbital engineering has recently been a much-pursued path to enhance functionalities in solids.<sup>1,2</sup> This is particularly true for transition-metal oxides, where the intricate coupling among lattice, spin, charge, and orbital degrees of freedom can be used to generate and control quantum phenomena.<sup>3</sup> Examples of the successful implementation of orbital engineering are the control of the Mott transition in  $\text{VO}_2$  films,<sup>4</sup> stabilizing 3D charge order in a cuprate superconductor,<sup>5</sup> and the manipulation of spin–orbit torque.<sup>6</sup> Common approaches to controlling orbital occupation and order typically involve the growth of thin film heterostructures. In these heterostructures, orbital engineering is then established through strain,<sup>7</sup> spatial confinement,<sup>8</sup> symmetry breaking,<sup>9,10</sup> or charge transfer.<sup>11</sup>

Heteroepitaxial strain is the most widely used method to manipulate lattice distortions and the resulting orbital effects in transition-metal oxides. In 3d transition-metal  $\text{ABO}_3$  perovskites, such as the strongly correlated  $\text{LaNiO}_3$  (LNO), the hybridization between B-site 3d states and O 2p states can provide a strong coupling mechanism between structural and orbital degrees of freedom. In a cubic perovskite unit cell, the crystal field of the  $\text{BO}_6$  octahedra splits the 3d orbitals into  $e_g$  and  $t_{2g}$  bands. Strain-induced structural distortion of these octahedra can be used to shift orbital degeneracy. In the simplest case of a tetragonal unit cell distortion, the  $e_g$  band splits into  $d_{z^2}$  and  $d_{x^2-y^2}$  orbitals, analogous to the well-known Jahn–Teller effect. LNO exhibits a Ni 3d<sup>7</sup> electronic configuration with a half-filled  $e_g$  band which can be driven

toward the lower-lying  $e_g$  orbital with increased tetragonal distortion. Functionally, the application of compressive heteroepitaxial strain in LNO thin films has demonstrated that it is possible to induce out-of-plane orbital polarization that can generate an enhancement in oxygen evolution and oxygen reduction catalytic applications due to greater orbital interactions at the reaction surface.<sup>7</sup>

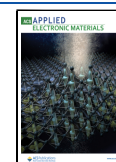
Standard thin film heterostructuring locks in a defined strain state and does not allow for postsynthesis control of the orbital occupation. However, thin film research as well as potential applications would largely benefit from the capability to fine-tune strain states and the ability to locally pattern strain states into a thin film. Strain doping has been developed as a method to address this need.<sup>12</sup> Here, postsynthesis low-energy He ion implantation is used to effectively induce a uniaxial out-of-plane lattice expansion. Previous work has demonstrated that strain doping can be applied to a large variety of materials where strain effects dominate defect-induced phenomena.<sup>13–16</sup> The uniaxial nature of strain doping makes it an ideal tool to manipulate the unit cell tetragonality of a film in a highly tunable and selective way that enables the direct study of strain

Received: April 22, 2025

Revised: July 18, 2025

Accepted: July 20, 2025

Published: July 29, 2025



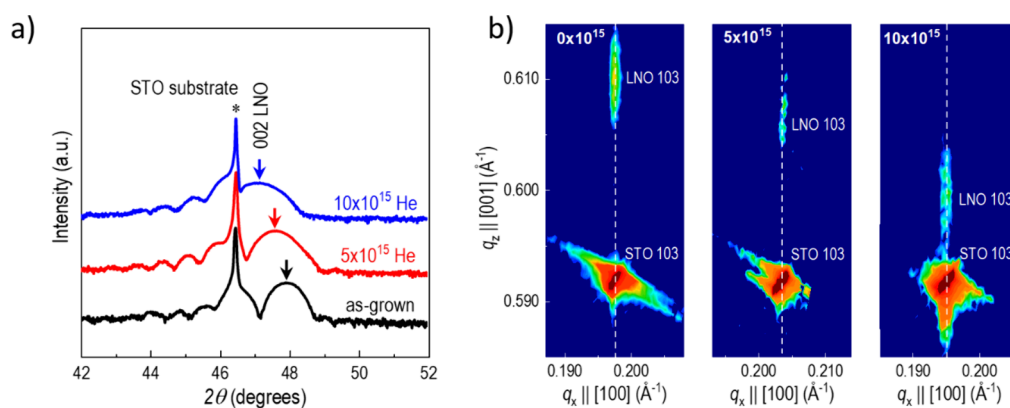


**Figure 1.** a) XRD  $\theta$ - $2\theta$  scan of the (002)<sub>pc</sub> peak of 12 nm LNO films on STO implanted with 0 to  $10 \times 10^{15}$  He/cm<sup>2</sup>. b) Reciprocal space maps around the (103)<sub>pc</sub> LNO peak for the three samples.

dependence on orbital occupation and the resulting functional properties. Prior works on  $\text{La}_{0.7}\text{Sr}_{0.3}\text{MnO}_3$  thin films used theoretical models to suggest uniaxial lattice expansion through strain-doping-induced changes to orbital occupation which could be manipulated to shift phase-transition temperatures and electronic phases.<sup>12</sup> However, experimental evidence of orbital states across implantations was not provided. Likewise, Wang et al. found a metal-insulator transition in He ion-implanted LNO films but did not measure or correlate these results with orbital polarization.<sup>17</sup>

In this work, we apply strain doping to epitaxial LNO films. Using X-ray spectroscopy, we provide direct proof that uniaxial strain induced by ion implantation changes the orbital occupancy of Ni 3d  $e_g$  states. The results are in good qualitative agreement with density functional theory. Comparing the effects of strain doping on uniaxial out-of-plane lattice expansion with as-grown heteroepitaxial biaxial in-plane strain demonstrates that unit cell tetragonality can be manipulated and used to shift the orbital polarization of the nickelate film. As a functional demonstration, oxygen reduction reaction measurements are conducted, which show that the change in orbital polarization leads to strongly enhanced catalytic activity, surpassing the improvements that can be achieved by epitaxial in-plane strain alone.

## RESULTS AND DISCUSSION

Three epitaxial (001)-oriented LNO films (12 nm thickness) were deposited by pulsed laser deposition on  $\text{TiO}_2$ -terminated  $\text{SrTiO}_3$  (001) substrates. Two of these films were then implanted postsynthesis with 4 keV He ions and fluences of  $5 \times 10^{15}$  and  $10 \times 10^{15}$  He/cm<sup>2</sup>. As seen by the presence of thickness fringes in the X-ray diffraction (XRD)  $\theta$ - $2\theta$  scans in Figure 1a, the as-grown films are deposited with a high structural film quality. The reciprocal space map in Figure 1b demonstrates that as-grown films are coherently strained to the lattice of the substrate. The in-plane strain is about 1.7%. The elastic reaction of LNO leads to an out-of-plane strain of -1.2% compared to that of the bulk lattice. The consequent pseudocubic unit cell tetragonality  $t = c/a$  is 0.971.

Under He ion implantation, the (002) XRD peak of the LNO film shifts toward lower  $2\theta$  values. This shift is a result of the out-of-plane lattice expansion induced by strain doping. The reciprocal space maps demonstrate that during this elongation the in-plane parameters of the films remain fixed to the substrates; i.e., the lattice expansion is uniaxial and directed

only along the out-of-plane direction. For the  $10 \times 10^{15}$  He/cm<sup>2</sup> dosed film, the uniaxial expansion compared to that of the as-grown film is 1.6%. This also means that the unit cell tetragonality is enhanced from 0.971 to nearly cubic 0.987. We note that the thickness fringes remain largely intact. This fact suggests that defect creation during the ion implantation process is rather small and that changes to the thin film properties can be mainly attributed to strain effects. See the Supporting Information for a *Stopping and Range of Ions in Matter* (SRIM-2013) calculation of the He ion distribution over the LNO heterostructure.

Linear dichroism through X-ray absorption spectroscopy (XAS) was used to characterize the evolution of the orbital occupation under ion implantation. Figure 2a shows

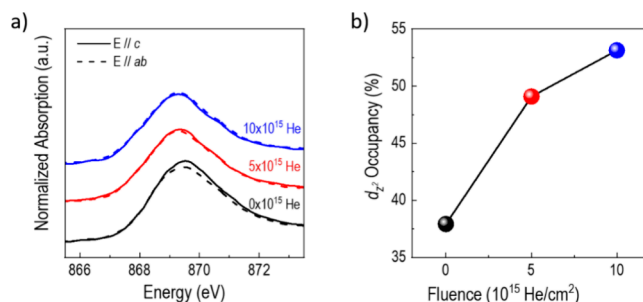


**Figure 2.** a) XAS spectra of the Ni L2 peak for LNO films on STO after increasing the out-of-plane lattice parameter with increased He implantation. The absorption along the  $c$ -axis ( $ab$ -axis) corresponds to holes in the  $d_{z^2}$  ( $d_{x^2-y^2}$ ) orbital. b) Occupation of the  $d_{z^2}$  determined by integration of XAS spectra and the application of sum rules. A trend toward enhanced  $d_{z^2}$  orbital occupation is seen with increasing ion dose.

absorption spectra on the Ni-L<sub>2</sub> edge for X-rays polarized both perpendicular ( $E//c$ ) and parallel ( $E//ab$ ) to the film plane. These spectra probe the energies and unoccupied states of the  $d_{z^2}$  and orbitals, respectively. We note that for all three films there is no shift in the polarization-averaged edge, indicating no observable deviation from stoichiometric  $\text{Ni}^{3+}$  due to oxygen defect generation under ion irradiation. Also, the XRD rocking curves shown in the Supporting Information do not show broadening of the LNO film peaks, which would be a signature of a substantial concentration of implantation-induced point defects. We conclude that although ion implantation naturally will create lattice defects they are not

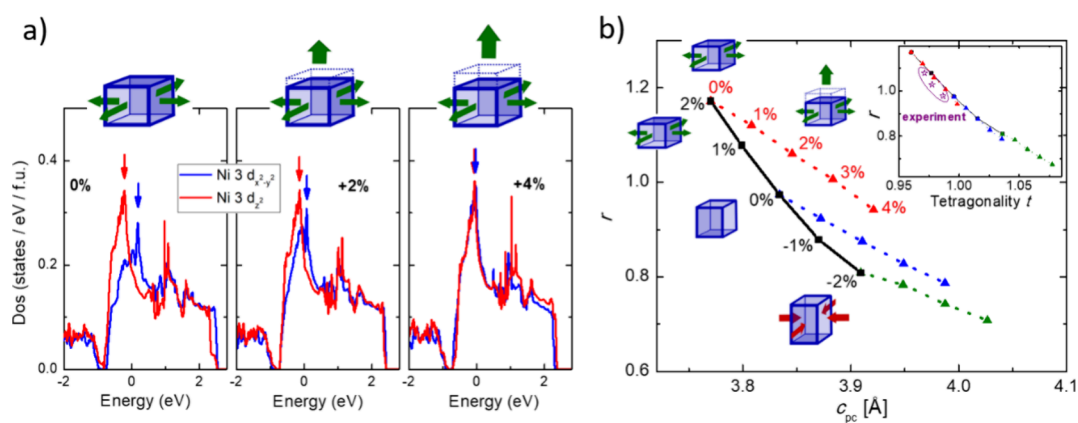


**Figure 3.** a) Orbital-density of states for the two Ni 3d  $e_g$  orbitals under a fixed tensile in-plane strain of 2%, but different uniaxial out-of-plane strain. b) Calculated hole ratio  $r$  under biaxial in-plane strain (black solid line) and uniaxial out-of-plane strain (colored dotted lines) as a function of the pseudocubic out-of-plane lattice parameter. The inset shows the same data as a function of the unit cell tetragonality. The experimental data was added to this figure.

the main driver for the changes to the linear dichroism described below.

For the as-grown film, the peak position and intensity of the  $E//ab$  curve are smaller than those of  $E//c$ . This observation is in agreement with previous work on the effect of epitaxial strain and is a result of orbital polarization shifting toward the  $d_{x^2-y^2}$  orbital under tensile in-plane strain<sup>7,18</sup> and other nickelates.<sup>19</sup>

We find that uniaxial out-of-plane strain reverses this trend. For the  $5 \times 10^{15}$  He/cm<sup>2</sup> film, both absorption spectra are almost identical, indicating a nearly vanishing difference in orbital occupation. The  $E//c$  spectra of the  $10 \times 10^{15}$  He/cm<sup>2</sup> film have a slightly smaller peak position and intensity than the  $E//ab$  spectra. The orbital polarization is shifted toward the  $d_{z^2}$  orbital with uniaxial lattice expansion. Figure 2b shows the  $d_{z^2}$  orbital occupancy as a function of the He ion dose as calculated using sum rules.<sup>10</sup> The  $d_{z^2}$  occupancy is effectively shifted from about 36 to 53%. In the calculation, we assume a total  $e_g$  manifold occupancy of  $n_{eg} = 1$ , as has frequently been done for single-layer LNO films, such as in the work of Wu et al.<sup>20</sup> See the Supporting Information for more details. If a larger  $n_{eg}$  value is assumed, then the variation of the occupancy is smaller. However, our main message that the orbital polarization can be tuned by ion implantation is not affected. Strain doping counteracts the depopulation of the  $d_{z^2}$  orbital induced by tensile biaxial strain by increasing the unit cell volume along the out-of-plane direction.

To further isolate the effect of uniaxial strain, we have performed density functional theory (DFT) calculations of LNO under biaxial in-plane and uniaxial out-of-plane strain. Figure 3a shows the partial orbital-resolved density of states (PDOS) near the Fermi energy for the  $d_{x^2-y^2}$  (blue) and the  $d_{z^2}$  (red) orbitals. The PDOS spectra are shown for three different strain states. All three structures are strained in plane by 2% and then superimposed on uniaxial out-of-plane strains of 0, 2, and 4%. This procedure mimics the effects of strain doping of a film coherently grown on SrTiO<sub>3</sub> substrates. The as-grown LNO model has a higher  $d_{z^2}$  PDOS slightly below the Fermi level but a lower PDOS above the Fermi level. However, when uniaxial strain is imposed, the difference between the  $d_{z^2}$  and  $d_{x^2-y^2}$  PDOS decreases and practically vanishes under 4% out-of-plane strain. This theoretical result suggests that uniaxial

strain has the opposite effect to tensile biaxial in-plane strain and is fully consistent with the experimental observations.

A quantity that can be determined by both DFT and XAS measurements and is independent of the correct choice of  $n_{eg}$  is the hole ratio  $r = h_{z^2}/h_{x^2-y^2}$ , where  $h_j$  is the number of holes in the orbital  $j$ .<sup>10</sup> In Figure 3b, we plot the theoretically calculated  $r$  as a function of the pseudocubic LNO out-of-plane parameter for different strain scenarios. The black solid line presents the result for compressive and tensile biaxial in-plane strain. A large tunability of the hole ratio is observed. For tensile strain, the hole ratio is  $>1$ , meaning that the Ni 3d  $d_{z^2}$  orbital is occupied with more holes than the  $d_{x^2-y^2}$  orbital; i.e., the  $d_{z^2}$  has an orbital occupation below 50%. Uniaxial out-of-plane strain, represented by dotted lines, lowers the hole ratio. This lowering happens regardless of the as-grown biaxial strain states of +2% (red), 0% (blue), and -2% (green). Interestingly, this predicts that it is likely possible to apply ion implantation to compressively grown thin films to push orbital polarizations into regimes currently inaccessible to heteroepitaxial strain.

In the LNO/SrTiO<sub>3</sub> case, uniaxial strain through He ion implantation counteracts the effect of tensile biaxial in-plane strain. The main reason for this observation is that uniaxial strain increases the tetragonality of the LNO unit cell and, in this scenario, pushes the film back toward a cubic state. The inset of Figure 3b shows the hole ratio  $r$  as determined from DFT calculations as a function of the unit cell tetragonality. A nearly linear relationship is observed, highlighting that the tetragonality of the perovskite unit cell is the dominant factor in tuning orbital polarization. Using the in-plane and out-of-plane lattice parameters determined from the XRD measurements shows good agreement between experimental and theoretical values. This result further corroborates that He ion implantation is driving the orbital occupation of the nickelate through uniaxial strain, rather than defect-related phenomena.

It was previously demonstrated that controlling orbital populations through heteroepitaxial strain is a powerful tool to improve the performance of catalytic active materials,<sup>21</sup> including LNO films.<sup>7</sup> Strain doping may thus be expected to provide a novel alternative means to finely tailor the catalytic activity. Figure 4a shows a measurement of the oxygen reduction reaction (ORR) as a function of the He ion fluence. We find a strong enhancement of the current densities when



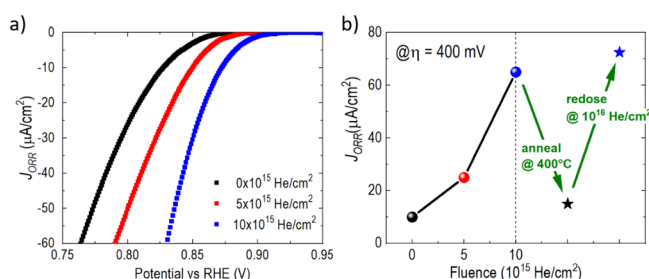


**Figure 4.** a) Polarization curves for the ORR for films implanted with different doses of helium. b) Current density at an overpotential  $\eta$  of 400 mV (ORR = 0.823 V). After implantation with  $10^{15}$   $\text{He}/\text{cm}^2$ , the film was annealed for 12 h at  $400^\circ\text{C}$  in a flowing oxygen atmosphere, remeasured (black star), redosed with  $10^{15}$   $\text{He}/\text{cm}^2$ , and consequently remeasured again (blue star).

increasing fluence. This increase is in qualitative agreement with the previous study on biaxial in-plane strain, where in-plane compression and the consequent enhanced unit cell tetragonality lead to a significantly enhanced ORR reaction as a result of increased  $d_z^2$  occupancy.<sup>7</sup> As expected, the as-grown LNO film's ORR response is measured to be nearly identical to that reported for the LNO film grown on STO. However, while the previous work demonstrated an increase in reactivity by inducing static tetragonality using heteroepitaxial compressive strain induced by a  $\text{LaAlO}_3$  substrate, the present work shows that increases in reactivity can be induced in a continuous manner on the tensile grown film without the need to change substrate. This trend not only supports the previous work's assertion that increasing out-of-plane orbital populations is a means of increasing ORR but also suggests that moving toward an artificially large unit cell volume not limited by the traditional Poisson effect may allow further enhancements to reactivity. There a clear increase in ORR with increasing uniaxial lattice expansion, and the ORR measured at the highest strain doping boosts the current density at an overpotential of 400 mV by almost a factor of 7 from  $\sim 10$  to  $\sim 65$   $\mu\text{A}/\text{cm}^2$  (Figure 4b), which is nearly twice the relative measured change achieved by epitaxy alone.<sup>7</sup> Interestingly, the strain doping effect is almost fully reversible when the He atoms are thermally annealed out of the LNO film at  $400^\circ\text{C}$  in a flowing oxygen atmosphere (Figure 4b). It is worth noting that this example is given to provide evidence of the efficacy of strain doping in controlling a well-documented orbital-induced functional response. A more thorough study is required to fully quantify the limits of catalytic control through strain doping. However, the importance of this result is that large improvements in catalytic activity can be created postsynthesis in a room-temperature process that is compatible with virtually all thin film preparation technologies.

## CONCLUSIONS

We have demonstrated that uniaxial lattice expansion induced by strain doping is a highly effective method to tune the orbital polarization in LNO films. The successful application of strain doping to other material systems and the general nature of strain-induced orbital splitting suggest that this approach can be used on a wide range of transition-metal oxides. The ability to fine-tune orbital occupancy through the ion implantation dose is particularly interesting in cases where lifting or restoring orbital degeneracy plays an essential role and will be of fundamental importance to understanding and

controlling in other complex systems such as cuprate- or iron-based superconductors and topological insulators.<sup>22,23</sup> Importantly, ion implantation can be conducted locally through masking or directly focused ion irradiation, which opens many possibilities for monolithic device fabrication of emerging electronic and sensing applications.

## EXPERIMENTAL METHODS

**Heterostructure Growth.** Epitaxial LNO films (12 nm in thickness) were grown on various oxide substrates by pulsed laser deposition. The LNO growth temperature, oxygen partial pressure, laser fluence, and repetition rate were optimized at  $600^\circ\text{C}$ , 100 mTorr,  $1.5 \text{ J}/\text{cm}^2$ , and 10 Hz, respectively.

**He Ion Implantation.** After film growth, Au films of 15 nm thickness were deposited on top of the sample to serve as a buffer and neutralization layer for helium ion implantation. The sample was cut into smaller pieces, and various helium doses were implanted using a SPECS IQE 11/35 ion source at an energy of 4 keV. After implantation, the Au layers were mechanically removed. No gold could be detected on the film surface after removal (e.g., see AFM image in SI).

**X-ray Diffraction.** X-ray diffraction was carried out using a Panalytical X'Pert thin film diffractometer with Cu  $K\alpha$  radiation.

**XAS.** XAS measurements were performed at beamline 4-ID-C of the Advanced Photon Source at Argonne National Laboratory. The measurement data presented were taken in fluorescence mode.

**Density Functional Theory Calculations.** DFT calculations were performed using the Perdew–Burke–Erzenhoff (PBE) exchange–correlation functional and ultrasoft potentials as implemented in Quantum ESPRESSO (PWSCF v.6.4.1). A plane wave cutoff of 790 eV and a Hubbard  $U$  value of 4 eV on the Ni  $d$  states were employed for all calculations. Epitaxial strain was imposed by constructing a supercell of  $\sqrt{2} \times \sqrt{2} \times 2$  pseudocubic unit cells with bulk-like rhombohedral structure and fixing the in-plane strain to the desired strain. Internal structural parameters are then relaxed. In order to impose uniaxial strain, the out-of-plane lattice vector was elongated, and internal structural positions were again relaxed. For self-consistent calculations, a  $6 \times 6 \times 6$   $k$ -point was employed, while for band structure calculations a  $13 \times 13 \times 13$  mesh was used.

**Electrochemical Characterization.** The ORR characterization was performed at  $25^\circ\text{C}$  in a 150 mL solution of  $\text{O}_2$ -saturated 0.1 M KOH developed with Sigma-Aldrich KOH pellets and Milli-Q water. A three-electrode rotating disk electrode (RDE) setup was used with a Pt counter electrode and a standard calomel (SCE) reference electrode. Potential was applied via a Biologic SP-200 potentiostat at 5 mV/s, and the samples had a rotating speed of 1600 rpm. Ohmic losses due to the film and solution were determined via a high-frequency ( $\sim 100$  kHz) impedance measurement and subtracted from the applied potential to obtain  $iR$ -corrected currents. Before polarization curves were determined, the potential was cycled at least 50 times at a scan rate of 50 mV/s between  $-0.3$  and  $0.7$  V vs SCE to expose a stable surface under these ORR/OER conditions. Subsequent polarization curves were taken at a scan rate of 5 mV/s at 1600 rpm at least three times to ensure reproducibility. More details can be found in the Supporting Information of ref 7.

## ASSOCIATED CONTENT

### Supporting Information

The Supporting Information is available free of charge at <https://pubs.acs.org/doi/10.1021/acsaelm.5c00815>.

SRIM calculations, XRD rocking curves, AFM topography after Au gold removal, and determination of  $d_z^2$  occupancy using XLD (PDF)

## AUTHOR INFORMATION

### Corresponding Authors

**Andreas Herklotz** – *Institute for Physics, Martin-Luther-University Halle-Wittenberg, 06120 Halle, Germany*;  
 orcid.org/0000-0002-1545-131X; Email: herklotza@gmail.com

**Thomas Z. Ward** – *Center for Nanophase Materials Sciences, Oak Ridge National Laboratory, Oak Ridge, Tennessee 37830, United States*;  
 orcid.org/0000-0002-1027-9186; Email: wardtz@ornl.gov

### Author

**Jonathan R. Petrie** – *Materials Science and Technology Division, Oak Ridge National Laboratory, Oak Ridge, Tennessee 37830, United States*

Complete contact information is available at:  
<https://pubs.acs.org/10.1021/acsaelm.5c00815>

### Notes

The authors declare no competing financial interest.

## ACKNOWLEDGMENTS

This material was based on work supported by the U.S. DOE, Office of Science, Basic Energy Sciences, Materials Science and Engineering Division at Oak Ridge National Laboratory (synthesis and characterization). Analysis and conceptualization was conducted at the Center for Nanophase Materials Sciences (CNMS), which is a U.S. Department of Energy, Office of Science User Facility at Oak Ridge National Laboratory. A.H. was funded by the German Research Foundation (DFG, grant no. HE8737/1-1).

## REFERENCES

- (1) Cantoni, C.; Mitchell, J. E.; May, A. F.; McGuire, M. A.; Idrobo, J.-C.; Berlijn, T.; Dagotto, E.; Chisholm, M. F.; Zhou, W.; Pennycook, S. J.; Sefat, A. S.; Sales, B. C. Orbital Occupancy and Charge Doping in Iron-Based Superconductors. *Adv. Mater.* **2014**, *26* (35), 6193–6198.
- (2) Tang, G.; Xiao, Z.; Hong, J. Designing Two-Dimensional Properties in Three-Dimensional Halide Perovskites via Orbital Engineering. *J. Phys. Chem. Lett.* **2019**, *10* (21), 6688–6694.
- (3) Goodenough, J. B. Perspective on Engineering Transition-Metal Oxides. *Chem. Mater.* **2014**, *26* (1), 820–829.
- (4) Aetukuri, N. B.; Gray, A. X.; Drouard, M.; Cossale, M.; Gao, L.; Reid, A. H.; Kukreja, R.; Ohldag, H.; Jenkins, C. A.; Arenholz, E.; Roche, K. P.; Dürr, H. A.; Samant, M. G.; Parkin, S. S. P. Control of the Metal-Insulator Transition in Vanadium Dioxide by Modifying Orbital Occupancy. *Nat. Phys.* **2013**, *9* (10), 661–666.
- (5) Ruiz, A.; Gunn, B.; Lu, Y.; Sasmal, K.; Moir, C. M.; Basak, R.; Huang, H.; Lee, J.-S.; Rodolakis, F.; Boyle, T. J.; Walker, M.; He, Y.; Blanco-Canosa, S.; da Silva Neto, E. H.; Maple, M. B.; Frano, A. Stabilization of Three-Dimensional Charge Order through Interplanar Orbital Hybridization in  $\text{PrxY}_{1-x}\text{Ba}_2\text{Cu}_3\text{O}_{6+\delta}$ . *Nat. Commun.* **2022**, *13* (1), 6197.
- (6) Liu, W.; Liu, L.; Cui, B.; Cheng, S.; Wu, X.; Cheng, B.; Miao, T.; Ren, X.; Chu, R.; Liu, M.; Zhao, X.; Wu, S.; Qin, H.; Hu, J. Manipulation of Spin-Orbit Torque in Tungsten Oxide/Manganite Heterostructure by Ionic Liquid Gating and Orbit Engineering. *ACS Nano* **2023**, *17* (23), 23626–23636.
- (7) Petrie, J. R.; Cooper, V. R.; Freeland, J. W.; Meyer, T. L.; Zhang, Z.; Lutterman, D. A.; Lee, H. N. Enhanced Bifunctional Oxygen Catalysis in Strained  $\text{LaNiO}_3$  Perovskites. *J. Am. Chem. Soc.* **2016**, *138* (8), 2488–2491.
- (8) Vambold, N. O.; Sazhaev, G. A.; Leonov, I. V. Interplay Between Electron Correlations, Magnetic State, and Structural Confinement in  $\text{LaNiO}_3$  Ultrathin Films. *JETP Lett.* **2023**, *118* (12), 886–892.
- (9) Chen, H.; Qiao, Q.; Marshall, M. S. J.; Georgescu, A. B.; Gulec, A.; Phillips, P. J.; Klie, R. F.; Walker, F. J.; Ahn, C. H.; Ismail-Beigi, S. Reversible Modulation of Orbital Occupations via an Interface-Induced Polar State in Metallic Manganites. *Nano Lett.* **2014**, *14* (9), 4965–4970.
- (10) Disa, A. S.; Kumah, D. P.; Malashevich, A.; Chen, H.; Arena, D. A.; Specht, E. D.; Ismail-Beigi, S.; Walker, F. J.; Ahn, C. H. Orbital Engineering in Symmetry-Breaking Polar Heterostructures. *Phys. Rev. Lett.* **2015**, *114* (2), 026801.
- (11) Wang, J.; Liu, Y.; Hou, Z.; Wang, S.; Yao, S.; Gao, X.; Zhang, H.; Tang, Z.; Nie, K.; Xie, J.; Yang, Z.; Yan, Y.-M. Engineering Antibonding Orbital Occupancy for Enhanced Sodium-Ion Intercalation Kinetics in Transition Metal Oxides. *Adv. Funct. Mater.* **2024**, *34* (28), 2316719.
- (12) Guo, H.; Dong, S.; Rack, P. D.; Budai, J. D.; Beekman, C.; Gai, Z.; Siemons, W.; Gonzalez, C. M.; Timilsina, R.; Wong, A. T.; Herklotz, A.; Snijders, P. C.; Dagotto, E.; Ward, T. Z. Strain Doping: Reversible Single-Axis Control of a Complex Oxide Lattice via Helium Implantation. *Phys. Rev. Lett.* **2015**, *114* (25), 256801.
- (13) Herklotz, A.; Rus, S. F.; Balke, N.; Rouleau, C.; Guo, E.-J.; Huon, A.; KC, S.; Roth, R.; Yang, X.; Vaswani, C.; Wang, J.; Orth, P. P.; Scheurer, M. S.; Ward, T. Z. Designing Morphotropic Phase Composition in  $\text{BiFeO}_3$ . *Nano Lett.* **2019**, *19* (2), 1033–1038.
- (14) Herklotz, A.; Gai, Z.; Sharma, Y.; Huon, A.; Rus, S. F.; Sun, L.; Shen, J.; Rack, P. D.; Ward, T. Z. Designing Magnetic Anisotropy through Strain Doping. *Adv. Sci.* **2018**, *5* (11), 1800356.
- (15) Herklotz, A.; Wong, A. T.; Meyer, T.; Biegalski, M. D.; Lee, H. N.; Ward, T. Z. Controlling Octahedral Rotations in a Perovskite via Strain Doping. *Sci. Rep.* **2016**, *6* (1), 26491.
- (16) Herklotz, A.; Rus, S. F.; Ward, T. Z. Continuously Controlled Optical Band Gap in Oxide Semiconductor Thin Films. *Nano Lett.* **2016**, *16* (3), 1782–1786.
- (17) Wang, C.; Chang, C.-H.; Huang, A.; Wang, P.-C.; Wu, P.-C.; Yang, L.; Xu, C.; Pandey, P.; Zeng, M.; Böttger, R.; Jeng, H.-T.; Zeng, Y.-J.; Helm, M.; Chu, Y.-H.; Ganesh, R.; Zhou, S. Tunable Disorder and Localization in the Rare-Earth Nickelates. *Phys. Rev. Mater.* **2019**, *3* (5), 053801.
- (18) Choi, M.-J.; Kim, T. L.; Kim, J. K.; Lee, T. H.; Lee, S. A.; Kim, C.; Hong, K.; Bark, C. W.; Ko, K.-T.; Jang, H. W. Enhanced Oxygen Evolution Electrocatalysis in Strained A-Site Cation Deficient  $\text{LaNiO}_3$  Perovskite Thin Films. *Nano Lett.* **2020**, *20* (11), 8040–8045.
- (19) Wang, L.; Stoerzinger, K. A.; Chang, L.; Yin, X.; Li, Y.; Tang, C. S.; Jia, E.; Bowden, M. E.; Yang, Z.; Abdelsamie, A.; You, L.; Guo, R.; Chen, J.; Rusydi, A.; Wang, J.; Chambers, S. A.; Du, Y. Strain Effect on Oxygen Evolution Reaction Activity of Epitaxial  $\text{NdNiO}_3$  Thin Films. *ACS Appl. Mater. Interfaces* **2019**, *11* (13), 12941–12947.
- (20) Wu, M.; Benckiser, E.; Haverkort, M. W.; Frano, A.; Lu, Y.; Nwankwo, U.; Brück, S.; Audehm, P.; Goering, E.; Macke, S.; Hinkov, V.; Wochner, P.; Christiani, G.; Heinze, S.; Logvenov, G.; Habermeier, H.-U.; Keimer, B. Strain and Composition Dependence of Orbital Polarization in Nickel Oxide Superlattices. *Phys. Rev. B* **2013**, *88* (12), 125124.
- (21) You, B.; Tang, M. T.; Tsai, C.; Abild-Pedersen, F.; Zheng, X.; Li, H. Enhancing Electrocatalytic Water Splitting by Strain Engineering. *Adv. Mater.* **2019**, *31* (17), 1807001.
- (22) Yu, R.; Hu, H.; Nica, E. M.; Zhu, J.-X.; Si, Q. Orbital Selectivity in Electron Correlations and Superconducting Pairing of Iron-Based Superconductors. *Front. Phys.* **2021**, *9*, DOI: 10.3389/fphy.2021.578347.
- (23) Gao, F.; Peng, Y.-G.; Xiang, X.; Ni, X.; Zheng, C.; Yves, S.; Zhu, X.-F.; Alù, A. Acoustic Higher-Order Topological Insulators Induced by Orbital-Interactions. *Adv. Mater.* **2024**, *36* (23), 2312421.